JOURNAL OF MATERIALS SCIENCE 27 (1992) 6426–6436

Laser transformation of Pb–Sb, Pb–Ca and Pb–Sb–Sn–As alloys

N. B. DAHOTRE, M. H. McCAY, T. D. McCAY
Center for Laser Applications, The University of Tennessee Space Institute, Tullahoma, TN 37388, USA

M. M. KIM
International Lead Zinc Research Organization Inc., Research Triangle Park Raleigh, NC 27709, USA

The laser treatment of the conventional battery grid alloys such as lead–calcium, lead–antimony and lead–antimony–tin–arsenic alloys was performed to improve mechanical, creep, and corrosion properties. The associated high cooling rate and increased solid solubility produced refined microstructures with unconventional and nonequilibrium phases. These effects resulted in an increase in the ultimate tensile strength, yield strength and modulus of elasticity and a decrease in elongation at fracture. Hardness of the laser-treated lead alloys was also increased substantially. Creep tests conducted under the conditions of constant load (1 kg) and temperature (25 °C) showed a large improvement in the creep resistance compared to that of the as-received lead alloys. Laser-surface treatment of lead–calcium and lead–antimony appears to decrease the weight-loss compared to as-received alloys during potentiostatic corrosion tests. The degree of the weight-loss varied for different alloys.

1. Introduction

Lead–acid storage batteries have been used for many years as starter batteries for internal combustion engines. The lead plates used for this purpose have to conduct the electric current while at the same time maintaining a uniform current distribution throughout the mass of this active material. If the current distribution is uneven, the changes in volume of the plates, during their charge and discharge, will be uneven, resulting in a tendency for the plate to buckle or crumble. In addition, the batteries are designed for long life during which the discharge is intermittent or extended over a long period of time. For such conditions, pure lead is too soft. As a result, extensive research efforts have been conducted [1, 2] to increase lead's mechanical strength, creep resistance and corrosion resistance (to extended periods of exposure to sulphuric acid) by standard alloying methods. During the past decades every element that has reasonable solubility and compatibility with lead has been tried [1], but of all the elements tried only a limited number of resulting alloys improved these properties for commercial application. They are antimonial, arsenical and calcium leads. Antimony presently, is a common alloying material and amounts up to about 11% have been employed to improve castability of the lead. Unfortunately, alloying elements such as antimony, tin, and arsenic, are relatively expensive. In addition, antimony increases the water loss of the battery and is of limited use in a maintenance-free battery [2]. Recently, attempts were made to solve these problems by reducing the amount of these elements in an alloy and, in some cases, by replacing these elements with inexpensive elements such as calcium and magnesium.

The strengthening mechanism in these alloys is a combination of precipitation and solution strengthening, precipitation hardening being more predominant in the antimonial–lead and calcium–lead alloys. Because both of these strengthening phenomena are due to nonequilibrium phase relationships [1], it would be expected that thermal and fabrication histories as well as ageing times would play a major role in the strength of lead products made from these alloys.

Another approach [1] to improving the properties of lead, was by dispersion strengthened by adding inert phases such as copper and/or PbO. Unfortunately, the excessive large sizes (44 μm) of these particles compared to precipitates produced by hardening heat treatment reduced the ductility of the material. Recently ASARCO Incorporated [2] developed a novel heat treatment to improve the strength of Pb–Sb–Cu–As–Se–Sn alloy. This process includes mechanical working followed by heating rapidly to the desired temperature and then quenching. Heat treatment of the alloy is performed under time and temperature conditions which do not result in a conventional solution treatment effect and the strengthening reaction occurring is not yet clear. This specific heat treatment is successful in only low per cent antimony and correlated arsenic–lead alloys.

Thus the road to improving several properties of lead by alloying and heat treatment has been often travelled in the past decades with many constraints and thereby with limited success. A completely new

0022–2461

method developed by the authors [3, 4] includes the treatment of lead and lead-alloy battery grid material using a high-power continuous wave CO_2 laser. This method utilizes the high power density available from a focused laser source to melt surface and subsurface material in an extremely short time. The focused laser beam enables very small volumes of the material to be melted at a given instant. Because the melting occurs rapidly and only in small volume, the bulk of the material remains cool, thus serving as an infinite heat sink. A large temperature gradient exists across the boundary between the melted and surrounding unmelted regions which results in rapid self-quenching and resolidification. A variety of chemical and microstructural states are retained because of rapid quenching from the liquid phase. These changes improved the mechanical and corrosion resistance properties. Thus, to understand better the effects of laser processing on lead alloys, the present study was undertaken.

2. Experimental procedure

The experimental approach involved laser melting the lead and lead alloys using a Rofin-Sinar (RS) 3000 laser. The RS3000 is a commercially available fast axial flow, RF (27.12 MHz) excited CO_2 (10.6 μm wavelength) gas laser. For the present experiment, the laser was operated in continuous mode. The processing parameters are given in Table I. The surface of the sample was melted by laying adjacent tracks with the beam focussed 25 mm above the surface of the workpiece. This provides a 2 mm wide melt track on the surface and almost complete melting through the thickness of the sample. The sample was laser treated on both sides to achieve uniform surface appearance. A computer numeric control system was used in conjunction with a five-axis Aerotech workstation to provide constant linear translation of the workpiece. During laser treatment, the sample was mounted on a workstation by sandwiching it between a water-cooled copper block substrate and another copper block with a window in it. This arrangement provided a high cooling rate in the sample and also prevented it from buckling due to thermal stresses developed during laser treatment. The compositions of the samples treated in this experiment are mentioned in Table II.

2.1. Tensile tests

Tensile testing was performed on as-received and laser-processed alloys using an Instron testing machine. To enable the use of small specimens and to avoid weight inertia effects due to the heavy grips on relatively soft lead and lead alloy samples, a specially made microtensile sample holder (Fig. 1) was used. The samples were flat with thickness of 1 mm. The gauge length was 25 mm. Each sample was loaded under uniaxial tension with the tensile axis parallel to the laser tracks on sample at a strain rate of $3.3 \times 10^{-4}\ s^{-1}$. The tensile tests were conducted at room temperature. Load–elongation curves were recorded on an X-Y recorder using the extensometer output. These were subsequently used to construct stress–strain curves from which ultimate tensile stress, UTS, yield strength, YS, elastic modulus, E, and elongation at fracture, e, were obtained.

TABLE I Laser processing parameters

Laser mode	Continuous wave CO_2 gas
Power delivered at work piece	1650 W
Beam mode	TEM_{10}
Beam polarization	Circular
Traverse speed	$100\ mm\ s^{-1}$
Focal position	25 mm above surface
Nozzle	Cross-flow nozzle for optics protection
Shielding gas	Argon, $4\ l\ min^{-1}$

TABLE II Compositions (wt %) of materials

Alloy	Sb	Ca	Sn	As	Pb
1	–	–	–	–	100
2	1.4	–	–	–	bal.
3	2.5	–	–	–	bal.
4	–	0.08	–	–	bal.
5	1.4	–	0.2	0.2	bal.
6	2.0	–	0.2	0.2	bal.

2.2. Creep tests

Creep testing was conducted in a specially designed temperature-controlled chamber. The chamber was a rectangular box ($90 \times 40 \times 36\ cm^3$) used for multiple sample testing. The temperature of the chamber was controlled by running water from a chiller through copper coils mounted on the inside walls. It was possible to control the temperature to within a $\pm 2\,^{\circ}C$ range. In the present experiment, creep tests were conducted at 25 °C. The creep-test samples had the same geometry and dimensions as those used for tensile tests. The sample was uniaxially loaded with 1 kg weight under static conditions. The deformation was recorded as an output of a resistance strain gauge (active tension gauge) mounted in the gauge section parallel to the tensile axis of the sample. An additional gauge (active compensation gauge) was mounted perpendicular to the tensile axis in the gauge section to compensate for the response to changes in temperature and compressive forces. The tension and compensation gauges were configured into the half-bridge Wheatstone circuit on the digital strain indicator unit (Model P-3500, Measurements Group, Inc.) which displayed the deformation as a microstrain. The readings were recorded at 8 h intervals initially followed by 24, 96 and 360 h intervals. A schematic drawing of the creep-test sample configuration for a single sample is shown in Fig. 2.

2.3. Corrosion tests

The potentiostatic tests on as-received and laser-treated lead alloys were conducted for corrosion properties at the Central Laboratory of Yuasa Battery Co. Ltd, Japan. The samples were rectangular coupons

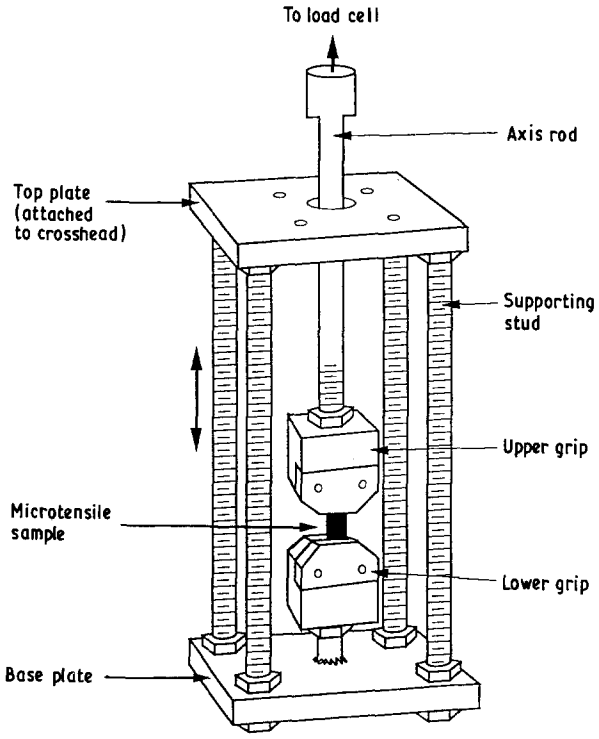

Figure 1 Schematic drawing of microtensile sample holder.

$(10 \times 2 \times 0.1\ cm^3)$. A schematic drawing of the experimental set-up is shown in Fig. 3 and the experimental parameters are mentioned in Table III. The samples were removed from the electrolyte after every 20 days for weight-loss, microstructural and X-ray diffractometry analyses. The potentiostatic tests were conducted for a total duration of 60 days.

2.4. X-ray diffractometry

A parallel set of experiments were conducted on as-received and laser-treated samples for X-ray diffractometry analysis. A Philips XRG3100 diffractometer with copper tube target (K_α radiation, 0.154 nm wavelength) was utilized for this purpose. The samples were scanned through 20°–100° for 2θ at a rate of $1°\ min^{-1}$. The results were plotted as intensity versus 2θ and the peaks obtained on these graphs were analysed for existing phases.

2.5. Metallography

For microstructural observations, the samples were fixed in cold resin and then prepared for longitudinal and cross-sectional views. The samples were etched with a mixture of glacial acetic acid (2 parts) and 30% H_2O_2 (1 part). The microhardness measurements were done with a 100 g load and Vicker's indentor.

3. Results and discussion

3.1. Microstructural evolution

Optical micrographs of as-received and laser-treated Pb + 0.08 % Ca, Pb + 1.4 % Sb and Pb + 1.4 % Sb + 0.2 % Sn + 0.2 % As are shown in Figs 4–6, respectively. At 300 °C, about 0.06 % Ca is soluble in lead, but at room temperature, the solubility drops to about 0.01 %, causing precipitation of Pb_3Ca. When Pb–Ca alloys containing more than 0.07 % Ca are solidified slowly, primary Pb_3Ca appears as cubes or blocks. Fig. 4a illustrates the occurrence of these Pb_3Ca precipitates (dark phase) in as-received Pb + 0.08 % Ca alloy. At the eutectic temperature of

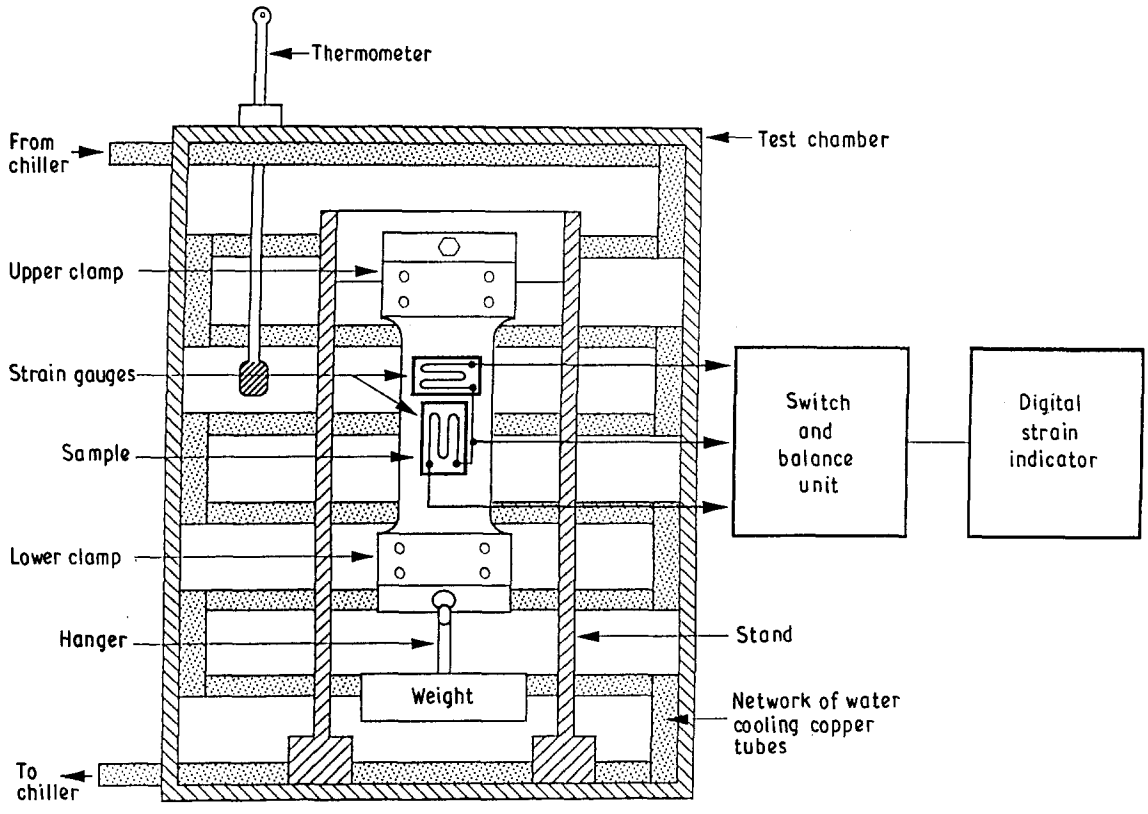

Figure 2 Schematic drawing of creep-test apparatus

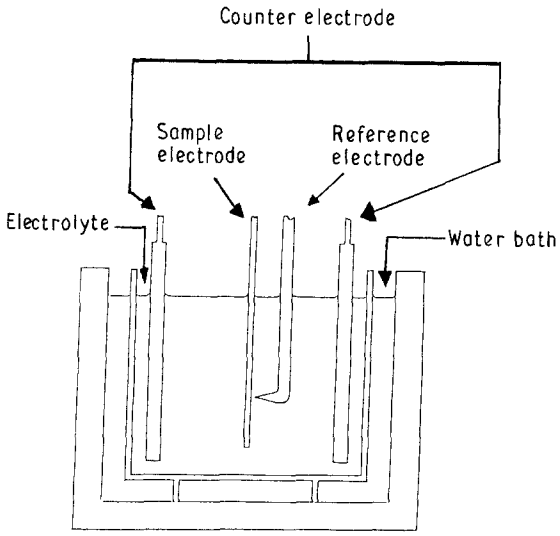

Figure 3 Schematic drawing of corrosion cell assembly.

TABLE III Corrosion (potentiostatic) test parameters

Electrolyte	1.285 sp. gr. H_2SO_4
Reference electrode	Hg/Hg_2SO_4
Counter electrode	Commercial lead–acid battery grid
Temperature of bath	50 °C
Test potential	1.35 V
Test duration	60 days

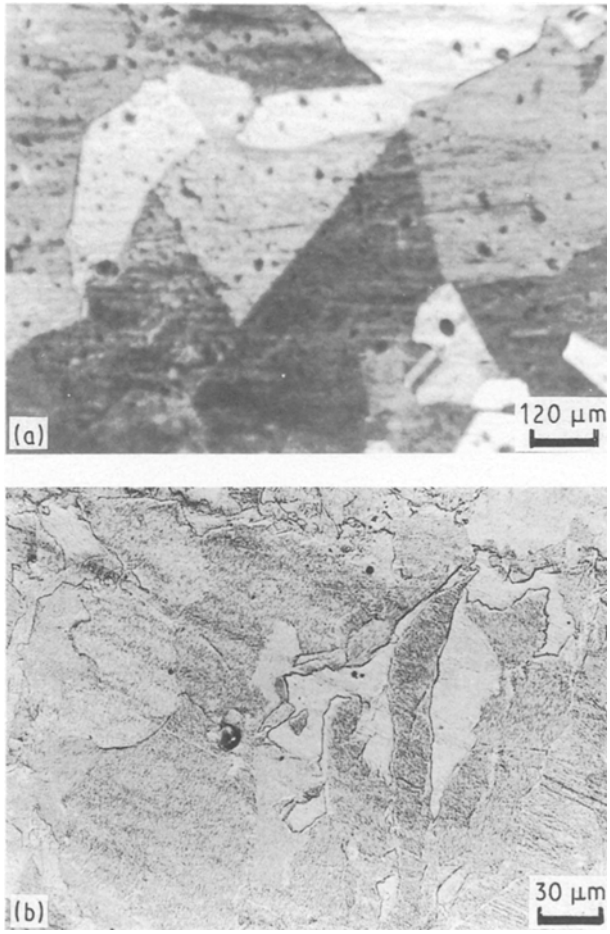

Figure 4 Microstructures of Pb + 0.08 wt % Ca alloy: (a) as-received, (b) laser-treated.

251 °C, 3.5 % Sb is soluble in lead, whereas at room temperature only 0.44 % Sb is soluble in lead. After cooling slowly, small rods of antimony precipitate from the solid solution and appear within the grains. The eutectic mixture has a lamellar form with particles of antimony (β-phase) in a matrix of lead-rich (α-phase) solid solution. In hypoeutectic alloys (below 11.2 % Sb), the α-phase of the eutectic blends into the primary lead-rich phase that is also present, giving the eutectic a divorced appearance. Fig. 5a shows such a microstructure of as-received Pb–Sb alloy. These are divorced structures with primary α dendrites (dark) and an interdendritic filling of eutectic (α + β). The white particles are β crystals. The Pb–Sb–Sn–As alloy system forms a ternary eutectic microstructure. One of the two peritectics in the Sb–Sn system occurs at 425 °C, where molten metal reacts with antimony-rich solid solution to form SbSn. Thus, as observed in Fig. 6a for as-received Pb–Sb–Sn–As alloys, the structure is a mixture of dark lead-rich grains and an intergranular lamellar ternary eutectic of Sb–Sn phase (light), antimony (light) and lead (dark). Arsenic dissolves in the lead and thus is not visible in the microstructure.

After laser treatment of the Pb–Ca alloy, the original cubes/blocks of Pb_3Ca precipitates reappear as extremely fine precipitates which are uniformly distributed within the grains (Fig.4b). The grain structure itself changed from polygonal to irregular grains and the relative size of the grains was reduced. In the case of the Pb–Sb alloys, the structure is extremely fine dendritic with an interdendritic network of antimony in a matrix of lead-rich solid solution (Fig. 5b). It is also clear from these photomicrographs that the higher content of antimony in the Pb–Sb alloys results in a smaller dendritic structure after laser treatment. The higher content of antimony changes the kinetics of solidification and offers a large number of nucleating sites [3, 4]. Similar effects were also observed in Pb–Sb–Sn–As alloys treated using a laser (Fig. 6b).

Thus the microstructures obtained in the laser-treated lead alloys (Figs 4b, 5b and 6b) are different from in the as-received lead alloys (Figs 4a, 5a and 6a). According to some researchers [5], the rapid solidification process such as in laser processing (cooling rate $> 10^5\,°C\,s^{-1}$) can produce large undercoolings below the liquidus temperature. Thermally, it causes the eutectic reactions in lead-alloys to occur at a temperature several degrees below that shown in the equilibrium diagrams. Structurally, it causes a refinement of the particle size of the phases precipitating in the reaction. Also, the high rate of solidification associated with this process does not permit time for liquid diffusion. Thus the dynamic conditions of rapid solidification induce heterogeneous microstructures made of fine dendrites.

3.2. X-ray diffractometry analysis

The X-ray diffractometry analysis of as-received and laser-treated lead alloys (Fig. 7) illustrates the exist-

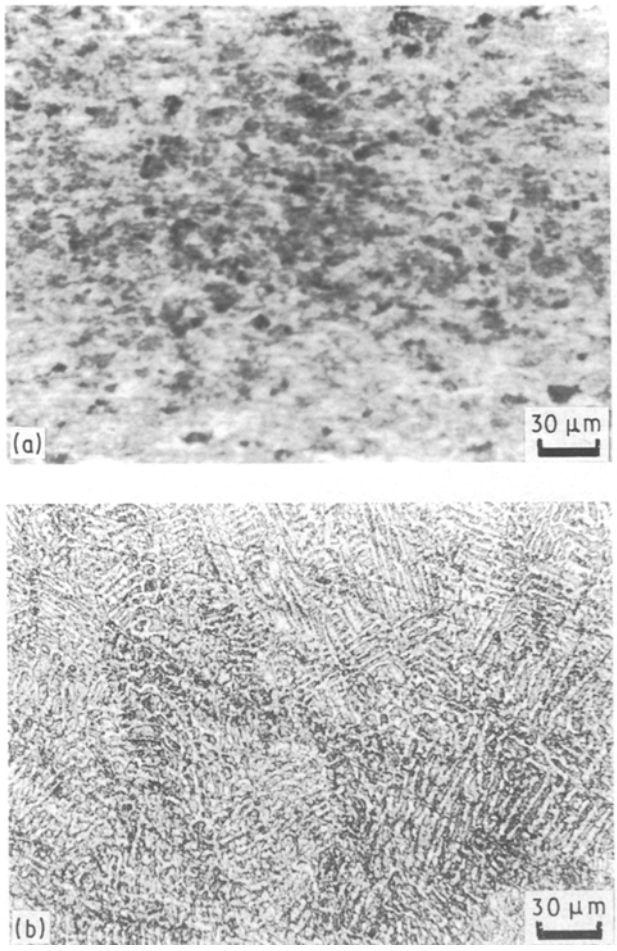

Figure 5 Microstructures of Pb + 1.4 wt% Sb alloy: (a) as-received, (b) laser treated.

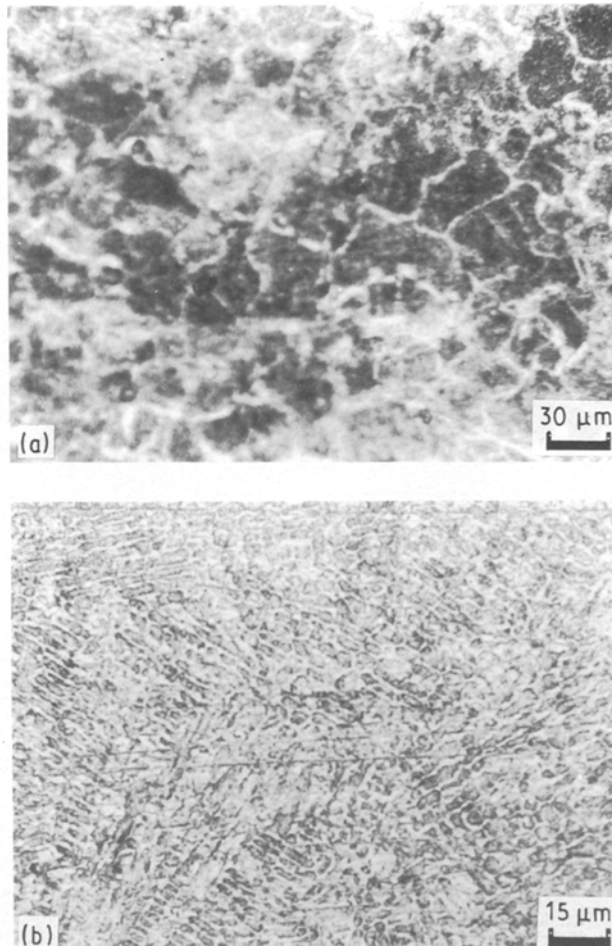

Figure 6 Microstructures of Pb + 1.4 wt % Sb + 0.2 wt % Sn + 0.2 wt % As alloy: (a) as-received, (b) laser-treated.

ence of several significant peaks which remained unidentified. These peaks and corresponding *d*-spacings (interplanar distances) do not match with existing standard phases referenced in the available literature [6]. In order to characterize these unidentified, unconventional phases formed during laser treatment, it is essential to use a technique such as transmission electron microscopy. Also, the volume of many phases formed during laser treatment of lead alloys are very small and, therefore, it was not possible to detect them by X-ray diffractometry technique.

Even though the surfaces of the samples were carefully cleaned for X-ray diffractometry studies, the presence of an oxide phase was noticed in all samples (Fig. 7), in ranges from diffraction angle (2θ) 23°–32°. This may be due to the surface oxidation or dispersion of oxide particles formed during earlier synthesis of the alloys. One cannot be sure about it at this stage and it requires more careful studies. The variation in the intensity on peaks of Pb (1 1 1) and Pb (2 0 0) is attributed to the grain-orientation effect.

3.3. Mechanical properties

The extremely fine precipitates produced during laser processing provide the pinning locations for dislocations. In addition, the evolution of unconventional and nonequilibrium phases and their distribution in the soft lead-rich phase matrix strengthens the material. These mechanisms together enhance the mechanical properties of the lead alloys processed with a laser. The effects are more evident in Table IV, which presents the tensile tests and hardness data on both as-received and laser-treated lead alloy samples. The values of UTS, YS and *E* are substantially higher for the laser-treated lead alloy samples than those of the untreated samples. As a result of the increase in the values of these parameters, the elongation at fracture for the laser-treated samples decreased by almost 50% below that for untreated samples. In spite of this lower elongation, however, it is still comparable to the value of elongation at fracture for pure lead. The hardness is higher for all laser-treated samples than for untreated samples, and it is about two to three times higher than for pure lead. These changes in the laser-treated lead alloy samples produce mechanically improved material for storage batteries.

3.4. Creep behaviour

Fig. 8 illustrates creep curve for pure lead and Fig. 9 shows creep curves for as-received and laser-treated lead alloys, respectively. The elongation occurring at the instant of loading, the instantaneous creep, consists mainly of elastic strain. The values of instantaneous creep for as-received lead alloys are lower than

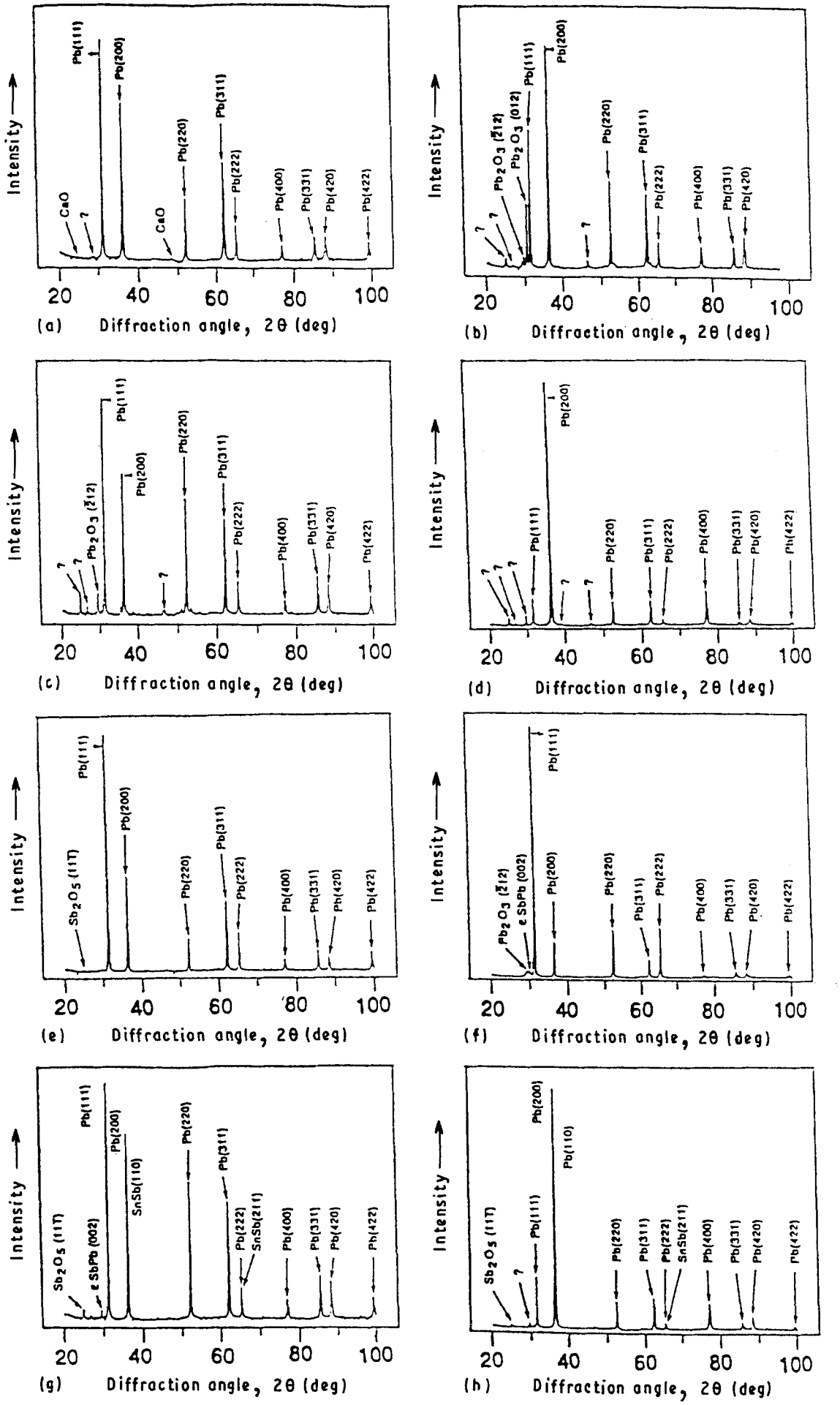

Figure 7 X-ray diffractometry data from lead alloys. (a, c, e, g, i) As-received, (b, d, f, h, j) laser treated. (a, b) Pb + 0.08 wt % Ca, (c, d) Pb + 1.4 wt % Sb, (e, f) Pb + 2.5 wt % Sb, (g, h) Pb + 1.4 wt % Sb + 0.2 wt % Sn + 0.2 wt % As, (i, j) Pb + 2.0 wt % Sb, + 0.2 wt % Sn + 0.2 wt % As.

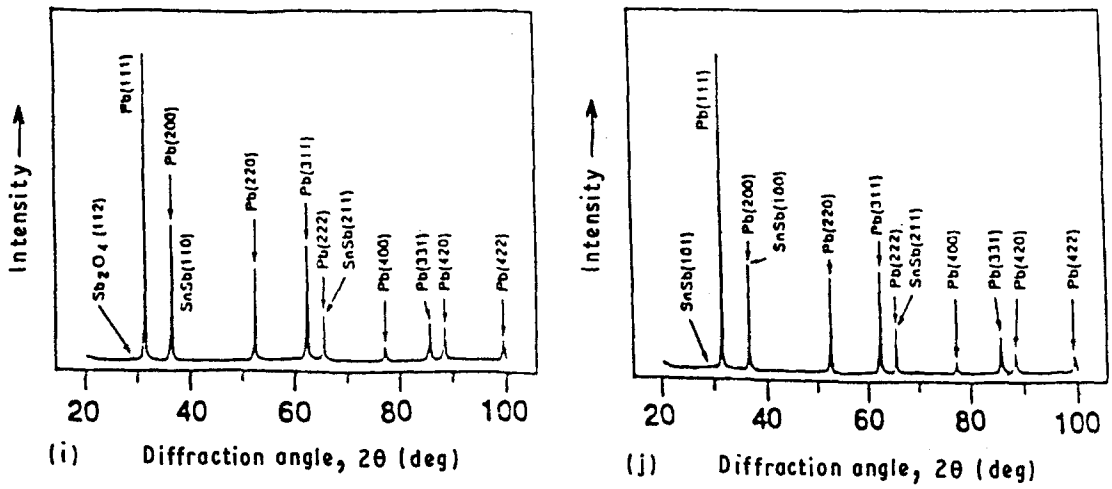

Figure 7 (Continued)

TABLE IV Tensile test and hardness data on lead and lead alloys

Alloy	Treatment	UTS (MPa)	YS (MPa)	E (MPa)	Elongation at fracture (%)	Vicker's hardness, 100 g ($kg\ mm^{-2}$)
1	As-received	12.84	3.85	2898	33	88
2	As-received	24.25	12.70	3174	51	125
	Laser-treated	33.88	19.32	3795	20	207
3	As-received	25.39	13.97	2415	49	227
	Laser-treated	36.75	29.39	4485	25	237
4	As-received	35.58	23.54	3243	36	110
	Laser-treated	42.16	27.50	5382	25	150
5	As-received	23.87	11.19	3174	47	148
	Laser-treated	33.81	17.60	4347	25	247
6	As-received	24.56	13.46	3519	49	135
	Laser-treated	39.95	22.47	4761	38	237

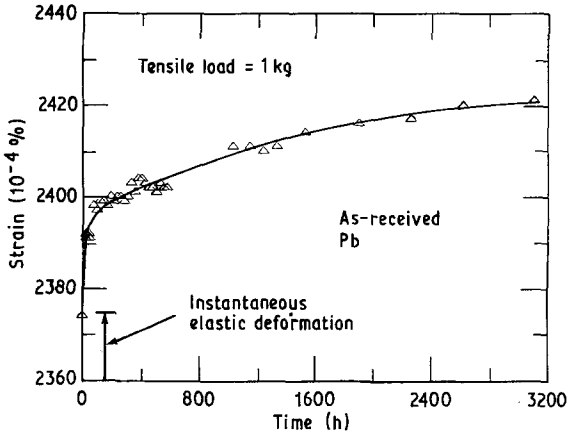

Figure 8 Creep curve for pure lead.

that for pure lead (2375×10^{-6}). The values of instantaneous creep for laser-treated lead alloys are about eight times lower than corresponding untreated alloys. The total primary creep (which follows instantaneous creep) values for laser-treated lead alloys are about eight to twelve times lower than those for untreated alloys. In some cases (Fig. 9a–e, and g) only primary creep was observed, indicating that the secondary creep was absent in these alloys.

The effect of alloying on creep behaviour is of great importance from the practical viewpoint because alloying is extensively used in creep-resistant commercial lead alloys. Because alloying elements are retained in solid solution, several interactions are possible, such as: elastic (Cottrell) interaction between stress field of a dislocation and the stress field caused by the misfit of solute atoms in the lattice; short- and long-range order interaction arising from the energy changes as order is destroyed by a moving dislocation; and chemical (Suzuki) interaction arising from the segregation of solute atoms to stacking faults of extended dislocation. These interactions play a role in the resistance of an alloy to recovery. As mentioned earlier and also observed in several earlier laser-materials interaction experiments [7–11], the rapid solidification rate produces large undercoolings below the liquidus temperature of alloys. When this occurs solidification takes place without rejection of the solute (in the present case, calcium, antimony, tin and arsenic) in the solvent (in the present case, lead). These solute atoms in solid solution are able to form atmospheres (Cottrell-type atmosphere) around moving dislocations. Thus creep rate in laser-treated lead alloys decreases rapidly because of the restraining action of the dislocations– atmosphere interaction.

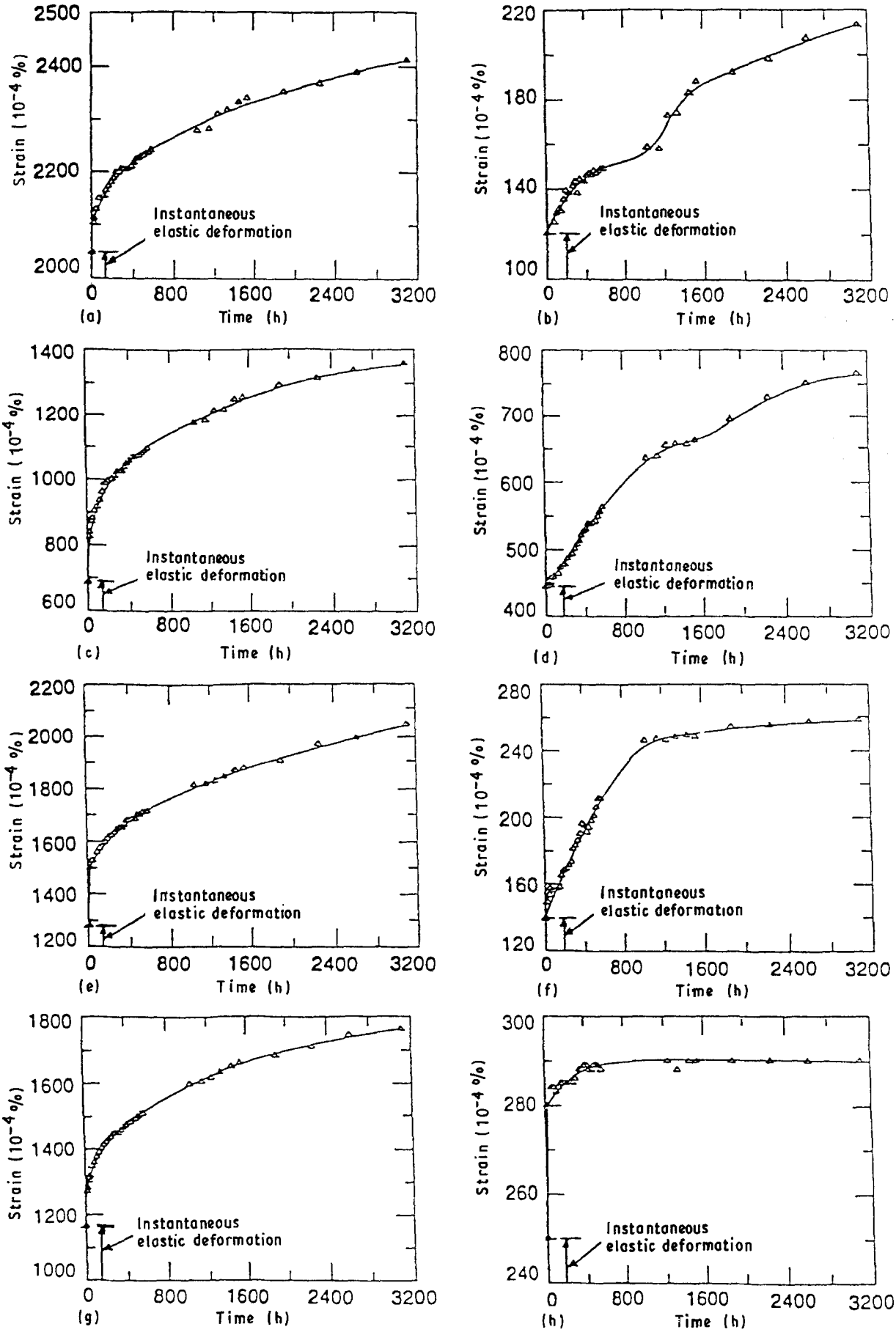

Figure 9 Creep curves for lead alloys, at a tensile load of 1 kg. (a, c, e, g, i) As-received, (b, d, f, h, j) laser-treated. (a, b) Pb + 0.08 wt % Ca, (c, d) Pb + 1.4 wt % Sb, (e, f) Pb + 2.5 wt % Sb, (g, h) Pb + 1.4 wt % Sb + 0.2 wt % Sn + 0.2 wt % As, (i, j) Pb + 2.0 wt % Sb, + 0.2 wt % Sn + 0.2 wt % As.

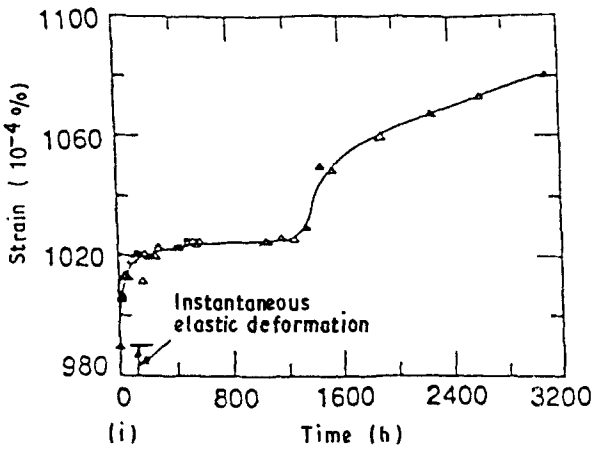

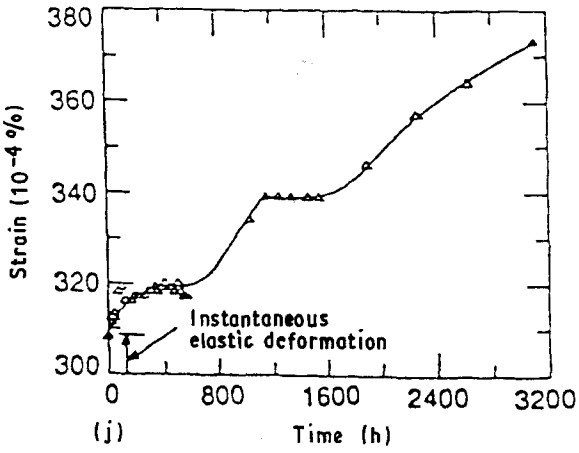

Figure 9 (Continued)

One of the microstructural factors known to affect primary and secondary creep is grain size. This effect is usually not large when compared to that of stress within normal ranges of grain sizes (10–1000 μm diameter) obtainable in polycrystalline metals and alloys [12]. But there are different observations quoted in this effect for many different alloys. Fe–Cr–Ni–Mn alloy tested under a constant tensile stress of 65 MPa at 704 °C showed an increase in the grain diameter from 9 μm to 82 μm decreased both primary and secondary creep rates [13]. For copper at 400 °C, the secondary creep increases with increasing grain diameter [14]. Finally, for tin at 25 °C, secondary creep decreases to a minimum as grain diameter increases and then increases as diameter is further increased [15]. In the present experiments, the laser processing involves very high cooling rate ($> 10^5$ °C s^{-1}) which, in turn, produced extremely fine grain structure (< 10 μm diameter) in the lead alloys. The change in grain structure of selected laser-treated lead alloys as compared to as-received lead alloys is shown in Figs 4–6. From these figures, together with Fig. 9, representing creep data, it can be concluded that the decrease in grain size of laser-treated lead alloys compared to that of as-received lead alloys produced a substantial decrease in total creep strain in laser-treated lead alloys during primary as well as secondary creep processes.

Primary and secondary creep of precipitation alloys (such as Ca–Pb and Sb–Pb) are also affected by particle size, distribution, volume fraction of the second phase and coherency stresses between particle and matrix [12]. In general, fine dispersions of precipitates or added insoluble particles increase creep resistance. Also, alloy systems (and heat treatment) that lead to the formation of a complex compound are usually more stable than binary compounds [12]. The laser treatment of alloys results in the formation of nonequilibrium metastable phases and fine structures. This process is also believed to modify the interface structures between matrix and particle. Such effects were recently observed in the laser-processed SiC particulate/aluminium alloy composites by the present authors [11]. These modifications enhanced the mechanical properties of the composite. Thus assuming the same effects occurred during laser treatment of lead alloys the enhanced creep resistance and mechanical properties are observed.

3.5. Corrosion behaviour

Fig. 10 shows the weight loss as a function of time in as-received and laser-treated Pb + 0.08% Ca and Pb + 2.5% Sb alloys. The topographical features of these alloys subjected to a potentiostatic test over a period of 60 days and after removal of the corrosion layers are illustrated in Fig. 11.

A remarkable difference in weight loss values between as-received and laser-treated Pb + 0.08% Ca was observed. The weight loss of the laser-treated sample was about 25% of that of the untreated sample over the period of testing (Fig. 10a). X-ray diffractometry analysis of the corrosion layer revealed the presence of mainly α-PbO_2. After removing the corrosion layer from an untreated Pb–Ca alloy, several craters were observed (Fig. 11a) which is an indication of pitting corrosion. On the other hand, in the case of laser-treated Pb–Ca samples, the corrosion appeared to progress via formation of cracks along the grain boundary (Fig. 11b). This is an intergranular corrosion.

The weight loss in untreated Pb + 2.5% Sb was greater than that in the laser-treated alloy (Fig. 10b) throughout the test period. The difference between the weight-loss values for untreated and laser-treated Pb + 2.5% Sb alloys was small compared to the weight loss difference in Pb + 0.08% Ca alloys. In both untreated and laser-treated samples of Pb–Sb the corrosion layer was mainly formed of α-PbO_2. β-PbO_2 was also present in the corrosion layer of the untreated sample. Corrosion of the as-received Pb–Sb alloy resulted in pitting on the surface (Fig. 11c). The laser-treated Pb–Sb alloy showed a few large diameter, shallow depth craters as an effect of the corrosion process (Fig. 11d). This effect was localized. Intergranular corrosion attack was also observed in laser-treated Pb–Sb alloys.

4. Conclusions

Laser treatment of conventional battery grid alloys (Pb–Ca, Pb–Sb and Pb–Sb–Sn–As) has demonstrated

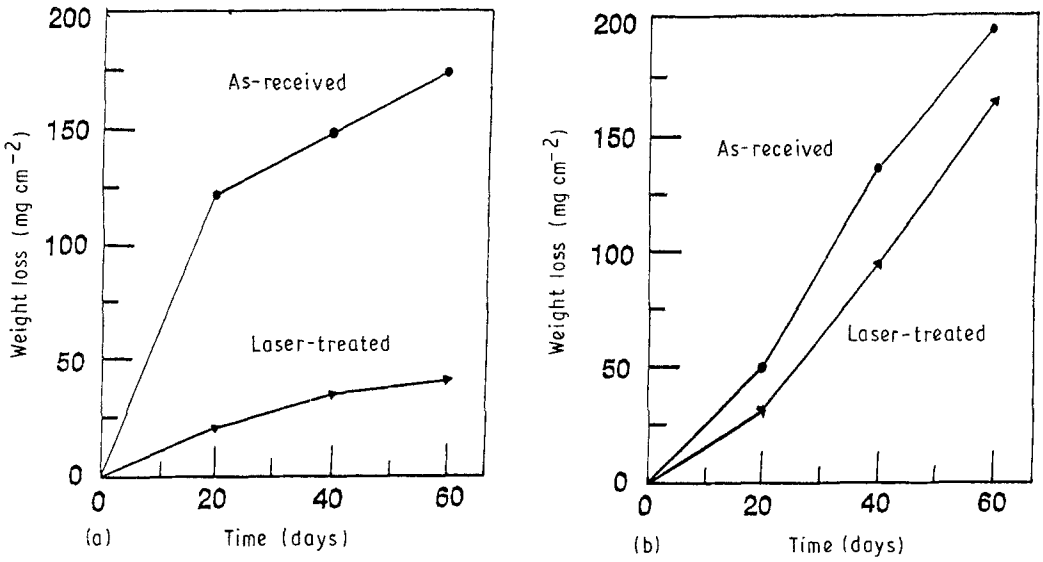

Figure 10 Weight loss–time curves for lead alloys: (a) Pb + 0.08 wt % Ca, (b) Pb + 2.5 wt % Sb.

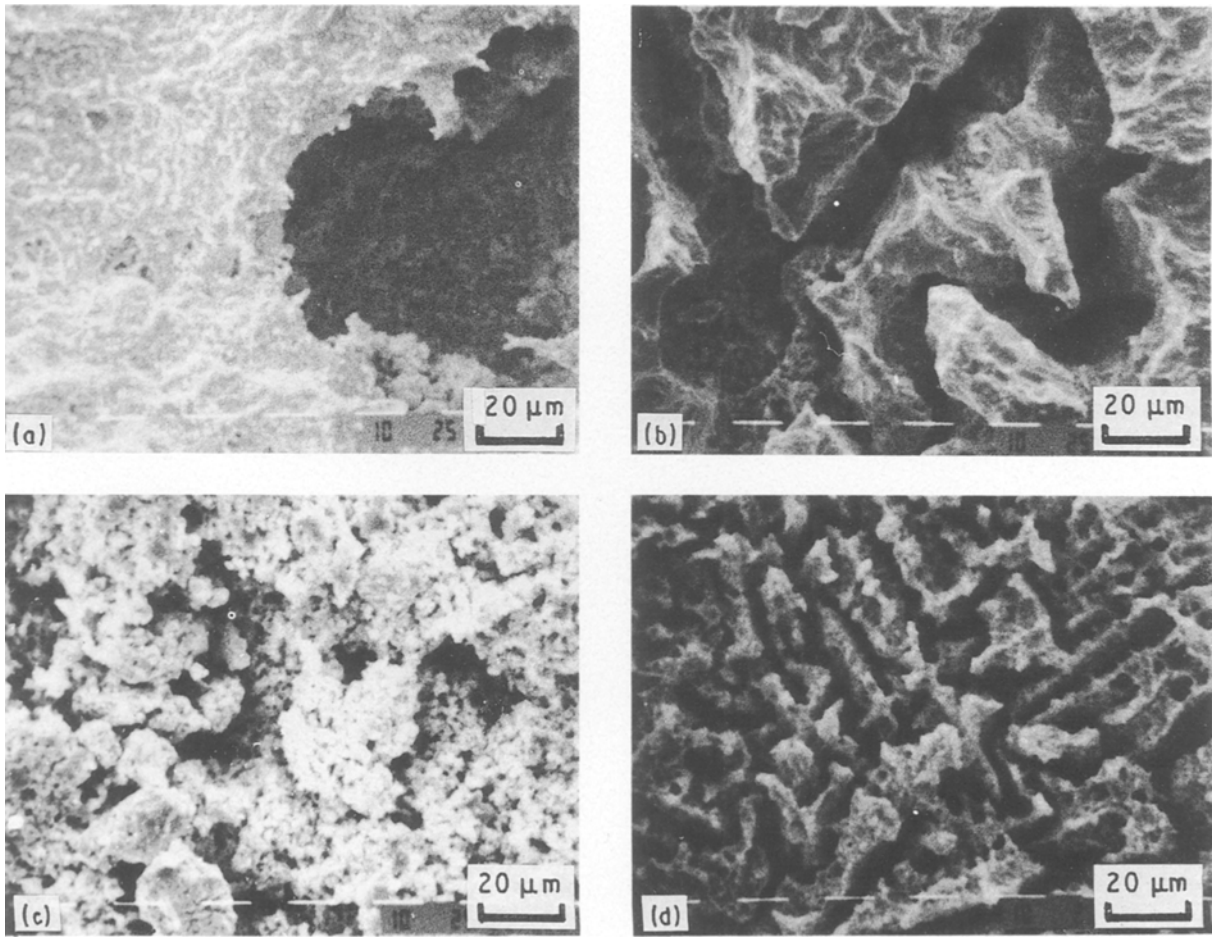

Figure 11 Scanning electron micrographs of lead alloys after removal of corrosion layer. (a, c) As-received Pb + 0.08 wt % Ca and Pb + 2.5 wt % Sb respectively. (b, d) Laser-treated Pb + 0.08 wt % Ca and Pb + 2.5 wt % Sb, respectively.

its ability to produce improved battery grids compared to untreated alloys. The extremely high cooling rate and increased solid solubility associated with laser processing produced microstructures with a heterogeneous distribution of unconventional and non-equilibrium phases. These changes enhanced mechanical properties (ultimate tensile strength, yield strength and modulus of elasticity) and also increased the hardness of the lead alloys. The laser process also improved the creep and corrosion resistance of the alloys. The values of instantaneous creep and primary creep for laser-treated lead alloys were much lower than those for corresponding as-received alloys. The corrosion test shows significant reduction in weight-loss in laser-treated lead alloys compared to the untreated alloys. The corrosion mode in as-received

alloys was pitting, whereas it was intergranular in laser-treated alloys. Based on these observations, laser processing of lead alloys holds great potential for battery-grid application.

Acknowledgements

This work was supported by the International Lead Zinc Research Organization, under Contract no. LE-395. The authors gratefully acknowledge the assistance of Michael Sharp in laser processing the material and Santosh Gopinathan and William Stephens in conducting the experiments.

References

1. H. E. HOWE, in "AIME Annual Meeting", 27 February–3 March 1966 (The Metallurgical Society of AIME, New York, 1966), Reprint no. 2A-RF-5.
2. M. MYERS, US Pat. 4 629 516, December 1986.
3. N. B. DAHOTRE, M. H. McCAY and T. D. McCAY, ILZRO Project LE-395, Progress Report no. 1, June 1990.
4. *Idem, ibid.*, Progress Report no. 2, December 1990.
5. M. COHEN, B. H. KEAR and R. MEHRABIAN, in "Proceedings of 2nd International Conference on Rapid Solidification Processing", edited by B. H. Kear, B. C. Giessen and M. Cohen, Reston, Virginia, March 1980 (Claitors Baton Rouge, LA, 1980) p. 1.
6. Powder Diffraction File (Inorganic Section), Vol. 1–40 (JCPDS International Center for Diffraction Data, PA, USA).
7. J. SINGH and J. MAZUMDER, *Met. Trans.* **18A** (1987) 313.
8. N. B. DAHOTRE and K. MUKHERJEE, *J. Mater. Sci.* **25** (1990) 445.
9. N. B. DAHOTRE, T. D. McCAY and M. H. McCAY, *J. Metals* **42** (6) (1990) 44.
10. N. B. DAHOTRE, T. D. McCAY and M. H. McCAY, *J. Appl. Phys.* **65** (1989) 5072.
11. N. B. DAHOTRE, M. H. McCAY, T. D. McCAY, S. GOPINATHAN and L. F. ALLARD, *J. Mater. Res.* **6** (3) (1991) 514.
12. F. GARAFALO, in "Fundamentals of Creep and Creep Rupture in Metals" (Macmillan, New York, 1966).
13. G. GAROFALO, W. DOMIS and F. GEMMINGEN, *Trans. AIME* **230** (1964) 1460.
14. E. R. PARKER, *Trans. ASM* **50** (1958) 52.
15. D. HANSON, *Trans. AIME* **133** (1939) 15.

Received 23 July
and accepted 28 November 1991